CMS Physics Analysis Summary

Contact: cms-pag-conveners-susy@cern.ch 2017/03/21

Search for direct production of bottom and top squark pairs in proton-proton collisions at $\sqrt{s} = 13$ TeV

The CMS Collaboration

Abstract

This note presents a search for direct production of bottom or top squark pairs in proton-proton collisions at a center-of-mass energy of $\sqrt{s} = 13$ TeV collected by the CMS experiment at the LHC in 2016. The data used correspond to an integrated luminosity of 36 fb^{-1}. This search is performed in a final state of two, three, or four jets accompanied by a significant imbalance in the transverse momentum. No statistically significant excess of events is found beyond the expected contribution from standard model processes. Exclusion limits are set in the context of simplified models of bottom- or top-squark pair production. Bottom squarks with masses below 1225 GeV are excluded at 95% CL for small values of the neutralino mass. Top squarks with masses below 525 GeV are excluded if the mass difference to the lightest neutralino is close to 10 GeV.

1 Introduction

The standard model (SM) has been extremely successful at describing particle physics phenomena. Nevertheless, it suffers from shortcomings such as the hierarchy problem [1–6], the need for fine-tuned cancellations of large quantum corrections to keep the Higgs boson mass near the electroweak scale. Supersymmetry (SUSY), based on a symmetry between bosons and fermions, is an attractive extension of the SM. A key feature of SUSY is the existence of a superpartner for every SM particle with the same quantum numbers, except for spin, which differs by one half unit. In R-parity conserving SUSY models [7, 8], supersymmetric particles are created in pairs, and the lightest supersymmetric particle (LSP) is stable [9, 10] and considered to be a candidate for dark matter [11]. Supersymmetry can potentially provide a "natural", i.e. not fine-tuned, solution to the hierarchy problem through the cancellation of quadratic divergences in particle and sparticle loop corrections to the Higgs boson mass. In natural SUSY models light top and bottom squarks with masses close to the electroweak scale are preferred.

This note reports on a search for pairs of SUSY particles produced in pp collisions at $\sqrt{s}$= 13 TeV at the LHC. The data used for this analysis correspond to an integrated luminosity of 36 fb^{-1} collected with the CMS experiment [12] during 2016. This search is performed using events with a large imbalance in the transverse momentum and two, three, or four jets among which one or two are identified as originating from bottom or charm quarks. This final state could originate from the decay of pairs of bottom ($\widetilde{\text{b}}$) and top ($\widetilde{\text{t}}$) squarks, where each $\widetilde{\text{b}}$ ($\widetilde{\text{t}}$) decays into a bottom (charm) quark and the lightest neutralino ($\widetilde{\chi}_1^0$), a weakly interacting neutral particle, as illustrated in Fig. 1. In the case of top squarks, only scenarios with a small difference between the $\widetilde{\text{t}}$ and $\widetilde{\chi}_1^0$ mass values are considered ("compressed" mass spectra), where the decay via a charm quark can be dominant [13]. In a large variety of models, the $\widetilde{\chi}_1^0$ is the lightest supersymmetric particle (LSP) and leaves the detector undetected, resulting in a characteristic signature of large missing transverse energy. The results of similar searches were previously reported by the ATLAS and CMS collaborations using proton-proton collisions at 7, 8 and 13 TeV [14–26].

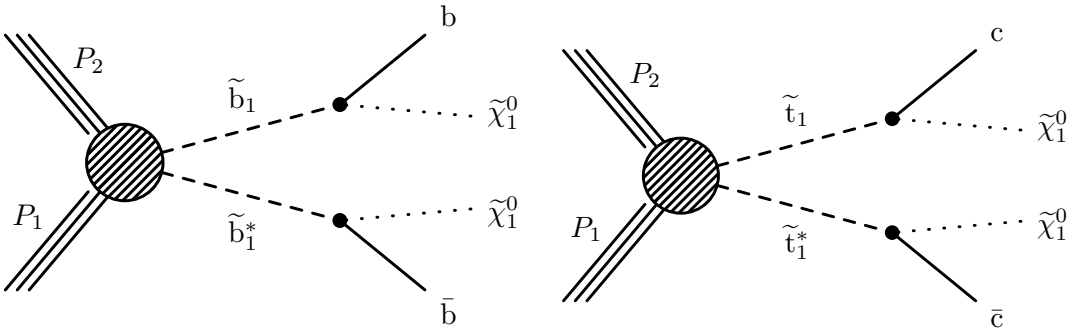

Figure 1: Diagrams showing the pair production of top or bottom squarks followed by their decays according to $\widetilde{\text{b}} \to \text{b}\widetilde{\chi}_1^0$ (left) and $\widetilde{\text{t}} \to \text{c}\widetilde{\chi}_1^0$ (right).

This note is organized in the following way. A brief review of the object reconstruction is given in Section 2, followed by the selection in Section 3. The various methods to estimate backgrounds due to standard model processes in the signal region are presented in Section 4. Section 5 summarizes the results and their interpretation in two different models as explained above.

2 Event Reconstruction and Monte Carlo simulation

Events are collected by a two-layer trigger system, based on a hardware filter (L1), followed by a software-based high level trigger (HLT). Events in the signal region are selected with a trigger that requires $E_{\mathrm{T}}^{\mathrm{miss}} > 100$ GeV, where $E_{\mathrm{T}}^{\mathrm{miss}}$ is calculated as the magnitude of the negative vectorial sum of the p_{T} of all particles at the trigger level. For events passing the analysis selection and having $E_{\mathrm{T}}^{\mathrm{miss}} > 250$ GeV, the trigger efficiency is found to be greater than 98%.

All final state observables used in this analysis are reconstructed using a particle flow (PF) algorithm [27–29], which combines information from various subdetectors to reconstruct and identify stable particles produced in the collision, namely charged and neutral hadrons, photons, electrons and, muons. These particles are clustered using the anti-k_{T} algorithm [30] with distance $\Delta R = \sqrt{(\Delta\eta)^2 + (\Delta\phi)^2} = 0.4$ to reconstruct jets. The contribution of neutral particles from overlapping pp interactions ("pileup") clustered into jets is subtracted based on the average pileup energy density in an event and the jet area calculated using FASTJET tools [31]. The jets are then corrected to take into account the detector response over the whole p_{T} spectrum and detector acceptance ($|\eta| < 5.0$). These corrections have been derived from Monte Carlo simulated events (MC) and validated using γ+jets and dijet events from collision data. In the end, the jets measured in data are corrected for any residual difference in energy scale between data and simulation [32].

Muons are reconstructed by finding compatible track segments in the silicon tracker and the muon detectors [33] and are required to be within $|\eta| < 2.4$. Electron candidates are reconstructed starting from a cluster of energy deposits in the electromagnetic calorimeter that is then matched to the momentum associated with a track in the silicon tracker. Electron candidates are required to have $|\eta| < 1.44$ or $1.56 < |\eta| < 2.5$. Muon and electron candidates are required to have p_{T} above 10 GeV and originate within 2 mm of the beam axis in the transverse plane. Lepton isolation is quantified as the sum of the p_{T} for particles within a cone of size ΔR around the lepton, normalized to the lepton p_{T}. The size of the cone is defined according to the lepton momentum, as in Eq. 1. The isolation sum is calculated using neutral and charged particle-flow candidates and is corrected for the effects of pileup.

$$\Delta R = \begin{cases} 0.2 & \text{if } p_{\mathrm{T}} < 50\,\mathrm{GeV} \\ 10\,\mathrm{GeV}/p_{\mathrm{T}} & \text{if } 50 < p_{\mathrm{T}} < 200\,\mathrm{GeV} \\ 0.05 & \text{if } p_{\mathrm{T}} > 200\,\mathrm{GeV} \end{cases} \quad (1)$$

The momentum imbalance vector ($\vec{p}_{\mathrm{T}}^{\mathrm{miss}}$) used in this analysis is calculated as the negative vector sum of transverse momenta of all the particle reconstructed in an event; its magnitude is referred to as $E_{\mathrm{T}}^{\mathrm{miss}}$.

Jets are identified as b-tagged jets using the combined secondary vertex (CSV) algorithm [34]. We use the "loose" and "medium" working point versions of this algorithm. The b quark identification efficiency for jets with p_{T} above 25 GeV and $|\eta| < 2.4$ is 80–85% and 46–74% for the loose and medium working points, respectively, and the rate for light quarks and gluons to be mistagged as b-tagged jets for the loose and the medium working points is 8–12% and 1–2%, respectively.

A c tagging algorithm is devised to identify jets from charm quarks, while rejecting either b or light jets [35]. Two algorithms are introduced, one to discriminate c jets from light jets (CvsL), and one for discriminating c jets from b-tagged jets (CvsB). To identify c-tagged jets, a selection

in the plane of the two discriminators is applied. The "medium" working point version of the algorithm has 40% c quark identification efficiency for jets with p_T above 25 GeV and $|\eta| < 2.4$. The rate for light quarks and gluons to be mistagged as a c quark is 20%.

Monte Carlo simulations are used to transfer background estimates from control to signal regions, to determine the yields for rare background processes, as well as to calculate the efficiency for various new physics scenarios. In this analysis, SM background samples and signal samples of squark pair production are generated with MADGRAPH V5 [36, 37] interfaced with PYTHIA V8.1 [38]. Standard model processes are simulated using a GEANT4-based model [39] of the CMS detector. The simulation of new physics signals is performed using the CMS fast simulation package [40]. All simulated events are processed with the same chain of reconstruction programs used for collision data. For both signal and background events, pileup interactions are simulated with PYTHIA and superimposed on the hard collisions, using a pileup multiplicity distribution that reflects the luminosity profile of the analyzed data. The object selection and identification efficiencies in simulation are corrected to match those measured in data.

3 Event selection

Selected events must have $E_T^{miss} > 250$ GeV and two, three, or four jets with $p_T > 25$ GeV and $|\eta| < 2.4$, passing loose requirements on the jet composition designed to reject noise and failures of the event reconstruction [41]. In the case of bottom squark production only two jets are expected from the squark decays. For the model involving top squarks with a small mass difference to the LSP, most decay products have small transverse momenta and the analysis uses the presence of one or two jets from initial-state-radiation (ISR). In both cases, the number of high-p_T jets is expected to be small and therefore, events having a fifth jet with p_T above 75 GeV are vetoed.

To reduce the background from SM processes with genuine E_T^{miss} arising from the decay of a W boson, we reject events having an identified electron or muon with $p_T > 10$ GeV. Only identified electrons (muons) with a relative isolation less than 0.1 (0.2) are considered in the veto. To suppress the background in which tau leptons decay to hadrons, we veto events containing one or more isolated tracks. The isolated track is obtained from a charged particle-flow candidate if it is identified as a PF hadron with $p_T > 10$ GeV, $|dz| < 0.1$ cm, and a relative track isolation of less than 0.1, where the relative track isolation is computed in a cone of size $\Delta R = 0.3$. After this requirement, residual background remains from $t\bar{t}$, single top, and W+jet events in which a W boson decays to a neutrino and a lepton failing the veto criteria. This lepton can be an electron or muon which is either out of detector, or kinematic acceptance, or misidentified, or a tau lepton that decays hadronically.

To suppress the background from SM multijet production we require that the minimum difference in azimuthal angle between the E_T^{miss} vector and each of the leading three jets ($\Delta\phi_{min}$) is greater than 0.4.

In order to increase the sensitivity across the bottom squark and LSP mass plane, we define two separate search regions, which we call the non-compressed and compressed regions. The non-compressed region covers the parameter space with large mass splitting ($\Delta m > 150$ GeV) between the bottom squark and LSP, while the compressed region is designed to increase the sensitivity in the parameter space with small Δm (< 150 GeV).

In addition to the baseline selection, events in the non-compressed region are required to have

a leading jet and second jet with p_{T} above 100 and 75 GeV, respectively, and if there is a third or fourth jet in the event, it must have p_{T} greater than 30 GeV. Both leading jets are required to be b-tagged. To keep the b-tag efficiency stable as a function of jet p_{T}, as well as to increase the signal to background ratio, two different b-tag working points are used to identify the leading b-tagged jet. The high-efficiency loose working point is used when the leading jet p_{T} is larger than 500 GeV. Otherwise, the medium working point with a lower mistag rate is used. The distribution of $\min M_{\mathrm{T}}(\mathrm{j}, E_{\mathrm{T}}^{\mathrm{miss}}) \equiv \mathrm{Min}[M_{\mathrm{T}}(\mathrm{j}_1, \vec{p}_{\mathrm{T}}^{\mathrm{miss}}), M_{\mathrm{T}}(\mathrm{j}_2, \vec{p}_{\mathrm{T}}^{\mathrm{miss}})]$, where $\mathrm{j}_1, \mathrm{j}_2$ are the two highest-p_{T} jets, is expected to have a kinematic endpoint at the mass of the top quark when $\vec{p}_{\mathrm{T}}^{\mathrm{miss}}$ and the closest jet originate from the semileptonic decay of a top quark. In the non-compressed search region we require $\min M_{\mathrm{T}}(\mathrm{j}, E_{\mathrm{T}}^{\mathrm{miss}})$ to be greater than 250 GeV.

We further characterize events using the kinematic variables H_{T} and m_{CT}. H_{T} is defined as the scalar sum of the transverse momenta of the two leading jets. The boost-corrected contransverse mass, m_{CT} [42, 43], is defined as:

$$\begin{aligned} m_{\mathrm{CT}}^2(j_1, j_2) &= [E_{\mathrm{T}}(j_1) + E_{\mathrm{T}}(j_2)]^2 - [\vec{p}_{\mathrm{T}}(j_1) - \vec{p}_{\mathrm{T}}(j_2)]^2 \\ &= 2p_{\mathrm{T}}(j_1)p_{\mathrm{T}}(j_2)(1 + \cos\Delta\phi(j_1, j_2)), \end{aligned} \tag{2}$$

Where $E_{\mathrm{T}}(j_i)$ is the energy and $\vec{p}_{\mathrm{T}}(j_i)$ is the 3-momentum vector of jet i (i = 1,2) and $\cos\Delta\phi$ is the azimuthal angle between two jets. For processes with two identical decays of heavy particles, $\widetilde{\mathrm{b}} \rightarrow j_i\, \tilde{\chi}_1^0$ the m_{CT} distribution is characterized by an endpoint defined by $m(\widetilde{\mathrm{b}})$ and $m(\tilde{\chi}_1^0)$, which for the topology in question is at $(m(\widetilde{\mathrm{b}})^2 - m(\tilde{\chi}_1^0)^2)/m(\widetilde{\mathrm{b}})$.

Events are categorized based on H_{T} and m_{CT} as shown in Table 1. The distributions of m_{CT} and H_{T} for all SM events and for a few signal points, after applying all selection requirements (non-compressed in Table 3), are shown in Fig. 2.

Table 1: The m_{CT} and H_{T} signal bins in the non-compressed search region.

Non-compressed						
H_{T} [GeV]	m_{CT} [GeV]					
[200,500]	[150,250]	[250,350]	[350,450]	> 450		
[500,1000]	[150,250]	[250,350]	[350,450]	[450,600]	> 600	
>1000	[150,250]	[250,350]	[350,450]	[450,600]	[600,800]	> 800

In the compressed region, events are required to contain high-p_{T} jets from ISR that can provide a transverse boost to the recoiling bottom and top squark systems, enabling such events to satisfy the trigger and selection conditions. Therefore, we require one or both hard jets and define the ISR-system according to whether one or both of two leading jets are b- or c-tagged.

The highest p_{T} jet must have $p_{\mathrm{T}} > 100$ GeV and must not be b- or c-tagged using the loose b-tagging and medium c-tagging working points, respectively. The p_{T} of the second jet has to exceed 25 GeV if it is b- or c-tagged, otherwise the threshold is set to 50 GeV. Here the medium operating points are used for both algorithms. There is a small possibility (less than 10%) that b-tagged jets are also identified as c-tagged jets, however due to the better b-tagging efficiency those jets are only counted as b-tagged jets and removed from c-tagged jets collection. The transverse momentum of the ISR system, defined as the two highest p_{T} jets that are neither b- nor c-tagged, is required to exceed 250 GeV.

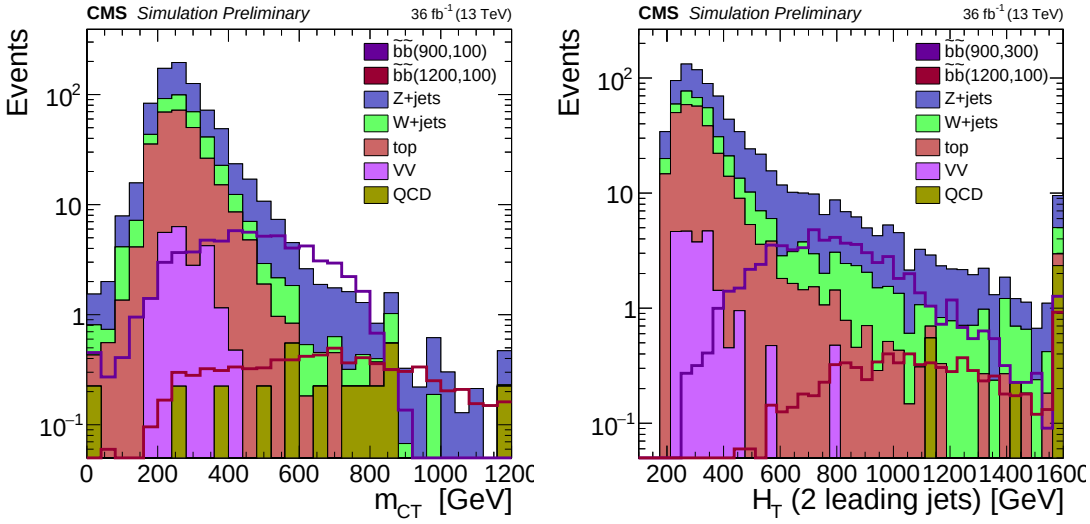

Figure 2: Distribution of m_{CT} (left) and H_{T} (right) for the search in the non-compressed region as obtained from simulation. The stacked, filled histograms represent different background components while the lines show three different model points for bottom squark production.

Although in this region the p_{T} requirement for b- and c-tagged jets is relaxed to 25 GeV, for the very compressed signals ($\Delta m < 25$ GeV) a large fraction of events contain b or c quarks with p_{T} below the 25 GeV which may fail to pass the jet selection or the b- or c-tagging working points. Therefore, we extend the identification of b and c quarks based on the presence of a secondary vertex (SV) reconstructed using the Inclusive Vertex Finder (IVF) algorithm [44]. To suppress the background originating from light quarks, the following requirements on the SV observables are applied: the distance in the transverse plane between the secondary and primary vertex (PV) must be less than 3 cm; the signed impact parameter significance with respect to the primary vertex is required to be greater than 4; the pointing angle, which is defined as $\cos(\overrightarrow{(\mathrm{SV},\mathrm{PV})}, \vec{p}_{\mathrm{SV}})$ must be greater than 0.98, where $\vec{p}_{\mathrm{SV}}$ is the total four-momentum of the tracks associated to the SV; the number of tracks associated with SV must be greater or equal to 3; in order to avoid overlaps with the b- and c-tagging selections describe above, the distance ΔR to any jet has to be greater than 0.4 and the transverse component of p_{SV} has to be lower than 25 GeV. The efficiency of b-hadron identification of the selected SV is around 50% versus 3% fake rate.

In the compressed region the jet imbalance in the transverse plane is quantified as the vector sum of the ISR-system p_{T} and $\vec{p}_{\mathrm{T}}^{\,\mathrm{miss}}$ with respect to $E_{\mathrm{T}}^{\mathrm{miss}}$ ($|(\vec{p}_{\mathrm{T}}(\mathrm{ISR}) + \vec{p}_{\mathrm{T}}^{\,\mathrm{miss}})|/E_{\mathrm{T}}^{\mathrm{miss}}$). For the topology of interest, the transverse momentum imbalance must be small and we therefore require that $|(\vec{p}_{\mathrm{T}}(\mathrm{ISR}) + \vec{p}_{\mathrm{T}}^{\,\mathrm{miss}})|/E_{\mathrm{T}}^{\mathrm{miss}}$ must be less than 0.5.

To increase the signal efficiency the search region is divided in signal regions based on number of b- or c-tagged jets ($N_{\mathrm{b-tags}}$ or $N_{\mathrm{c-tags}}$, respectively) and selected SV (N_{SV}), $E_{\mathrm{T}}^{\mathrm{miss}}$, H_{T} (b-tagged jets), and H_{T} (c-tagged jets) which are the scalar sum of b-tagged jets or c-tagged jets, respectively. The signal region definitions are shown in Table 2. The b-, c-tagged jet, and selected SV multiplicities for all events that pass the selection requirement shown in the third column of Table 3, and $E_{\mathrm{T}}^{\mathrm{miss}}$ distribution for the events with at least one b- or c-tagged jet are shown in Fig. 3.

Table 2: The signal bin definitions in the compressed search region.

compressed region		
N_{b-tags},N_{c-tags},N_{SV}	E_T^{miss} [GeV]	H_T (b- or c-tagged jets) [GeV]
N_{b-tags} =1	[250, 300]	<100
	[300, 500]	<100
	[500, 750]	<100
	[750, 1000]	<100
	>1000	<100
N_{b-tags} =2	[250, 300]	<100 [100, 200]
	[300, 500]	<100 [100, 200]
	>500	<100 [100, 200]
N_{c-tags} =1	[250, 300]	<100
	[300, 500]	<100
	[500, 750]	<100
	[750, 1000]	<100
	>1000	<100
N_{c-tags} =2	[250, 300]	<100 [100, 200]
	[300, 500]	<100 [100, 200]
	[500, 750]	<100 [100, 200]
	>750	<100 [100, 200]
N_{b-tags} +N_{c-tags} =0,N_{SV} >0	[250, 300]	-
	[300, 500]	-
	[500, 750]	-
	[750, 1000]	-
	>1000	-
N_{b-tags} +N_{c-tags} +N_{SV} =0	[300, 500]	-
	[500, 750]	-
	[750, 1000]	-
	[1000, 1250]	-
	>1250	-

4 Background Estimation

In this analysis, the main backgrounds fall into three categories:

- "Invisible Z": $Z \to \nu\nu$ events produced in association with jets that lead to genuine E_T^{miss} are the most signal-like of the background processes. This background is estimated primarily from a control sample of $Z \to \ell^+\ell^-$ events, as explained in Section 4.1.
- "Lost lepton": $t\bar{t}$ and $W+$jets production processes are the main contributions in this category and smaller contributions come from single top. These processes contribute to the search regions when the W boson decays leptonically providing a source of genuine E_T^{miss} from the neutrino. These processes are highly suppressed by rejecting events containing an isolated electron, muon, or a track as discussed in Section 3. However, events with an electron or a muon can contribute to the signal region when the lepton is not isolated or identified, or is out of kinematic or detector acceptance. In addition, a hadronically decaying tau lepton is reconstructed as a jet and hence contributes to the signal region. Together, these events are referred to as the lost lepton background. It is primarily estimated using a control sample of one-lepton events. Section 4.2 describes how this background is estimated.

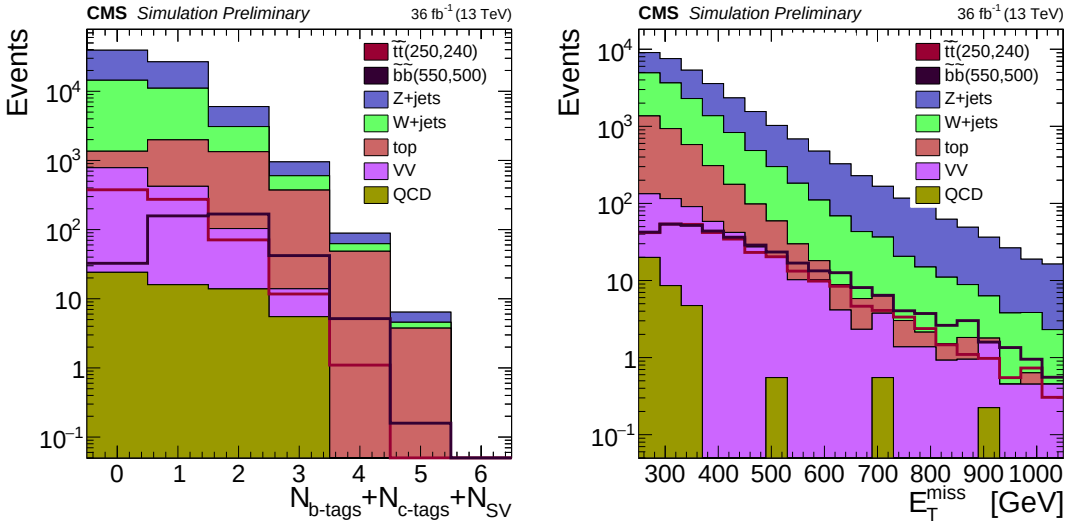

Figure 3: Distributions of the combined b-, c-tagged jet, and SV multiplicity (left), and $E_{\mathrm{T}}^{\mathrm{miss}}$ for events with at least one b- or c-tagged jet (right) after the baseline selection for the compressed region as obtained from simulation. The stacked, filled histograms represent different background components while the lines show three different model points for bottom squark production.

- "QCD": multijet events contain no genuine $E_{\mathrm{T}}^{\mathrm{miss}}$ and are strongly suppressed by the baseline selection. Any residual background comes from jet mismeasurement resulting in large experimental $E_{\mathrm{T}}^{\mathrm{miss}}$, Section 4.3 covers this background.

Small contributions are expected from other SM processes, including diboson production. They are estimated from simulation with 50% systematic uncertainty.

4.1 $Z \to \nu\nu$ estimation

This background is estimated from simulation after applying renormalization and shape correction factors that are determined from a data sample of $Z \to \ell^+\ell^-$ events in which the leptons are removed and all kinematic variables are re-calculated to emulate $Z \to \nu\nu$ events. Events are collected using a trigger that requires one or two muons or two electrons. For the single muon triggers, the muon must have p_{T} >50; for the double muon or electron triggers, the leading and second lepton must have $p_{\mathrm{T}} > 17$ GeV, 12 GeV, respectively. In the offline selection, we require that these events have two opposite charge and same flavor leptons with $p_{\mathrm{T}} > 25$ (20) GeV and $|\eta| < 2.4$, whose invariant mass is within 15 GeV of the mass of the Z boson [45]. Leptons are required to be separated from all jets in the event by $\Delta R > 0.3$. Aside from the lepton selection, the same object and event selection criteria described in Section 3 are applied to this sample. Selected events are further subdivided in both the non-compressed and compressed regions applying the selection described in Section 3.

The expected number of $Z \to \nu\nu$ events in each signal region bin is then obtained by scaling the signal region yield, $N^{MC}_{Z\to\nu\nu}$, by the renormalization factor and shape correction factor, according to Eq. 3.

$$N^{pred}_{Z\to\nu\nu}(SR) = N^{MC}_{Z\to\nu\nu} \frac{\mathrm{N}^{\mathrm{Data}}_{Z\to\ell^+\ell^-}}{\mathrm{N}^{\mathrm{MC}}_{Z\to\ell^+\ell^-}} \cdot \mathrm{S}_{\mathrm{Data/MC}} \tag{3}$$

Table 3: Baseline selections in both the non-compressed and compressed regions.

	Search Regions	
	Non-compressed	Compressed
N_{jets}	2, 3, 4 ($p_{\text{T}} > 30$ GeV)	2, 3, 4 ($p_{\text{T}} > 30$ GeV)
Jet veto	5th-jet ($p_{\text{T}} > 75$ GeV)	5^{th}-jet ($p_{\text{T}} > 75$ GeV)
Lepton veto	e, μ, and Isolated track	e, μ, and Isolated track
1^{st}-jet	$p_{\text{T}} > 100$ GeV, is b-tagged	$p_{\text{T}} > 100$ GeV, is not b- or c-tagged
2^{nd}-jet	$p_{\text{T}} > 75$ GeV, is b-tagged	$p_{\text{T}} > 25(50)$ GeV if is (not) b- or c-tagged
$E_{\text{T}}^{\text{miss}}$	>250 GeV	>250 GeV
p_{T} (ISR)	-	>250 GeV
$\Delta\phi_{\text{min}}$	>0.4	>0.4
$\lvert(\vec{p}_{\text{T}}(\text{ISR}) + \vec{p}_{\text{T}}^{\text{miss}})\rvert / E_{\text{T}}^{\text{miss}}$	-	<0.5
$\text{min}M_{\text{T}}(\text{j}, E_{\text{T}}^{\text{miss}})$	>250 GeV	-
H_{T}	(two leading jets)> 200 GeV	-
m_{CT}	> 150 GeV	-

where $N^{MC}_{Z\to\nu\nu}$ is the yield in the signal region predicted by simulation and $\frac{N^{\text{Data}}_{Z\to\ell^+\ell^-}}{N^{\text{MC}}_{Z\to\ell^+\ell^-}}$ is the renormalization factor for the dilepton selection after applying the b- and c-tagging requirements of the SR. The shape correction factor, $S_{\text{Data/MC}}$ accounts for possible differences in the shape of the observables used to define the signal regions. To compensate for the smaller yields for $Z \to \ell^+\ell^-$ compared to $Z \to \nu\nu$, b-tagged jets are selected using a looser working point for the non-compressed region and an inclusive $N_{\text{b-tags}}$, $N_{\text{c-tags}}$ and N_{SV} bin is used to extract the correction factor. The shape correction factor in the non-compressed region is determined via comparison of the m_{CT} distribution of the $Z \to \ell^+\ell^-$ in simulation and data. To do the comparison we first normalize the simulation to the number of observed events in data after applying the loose selection criteria. The small contamination from $\text{t}\bar{\text{t}}$, W+jets, single-top and diboson production is estimated using simulation and subtracted from data. After applying the shape correction factor in bins of m_{CT}, good agreement between the data and simulation is found as a function of $E_{\text{T}}^{\text{miss}}$ and H_{T}. A small residual difference in the shape of the H_{T} distribution is assigned as a systematic uncertainty. In addition to the shape correction factors, the normalization factor is calculated in the $Z \to \ell^+\ell^-$ control sample using the same b-tag requirement as signal region, and the value is determined to be consistent with one within the statistical uncertainty.

For the compressed region, the shape correction factors are calculated inclusively in $N_{\text{b-tags}}$, $N_{\text{c-tags}}$, and N_{SV} as a function of $E_{\text{T}}^{\text{miss}}$ in the same way as in the non-compressed region. The normalization factors are determined in each $N_{\text{b-tags}}$, $N_{\text{c-tags}}$, and N_{SV} signal region separately, and are consistent with unity within their statistical uncertainties.

Two sources of systematic uncertainties on the predicted $Z \to \nu\nu$ are considered: uncertainties associated with the use of simulation and uncertainties connected to the background prediction method itself. The first set of uncertainties are related to renormalization and factorization scale, parton distribution functions (PDFs), jet and $E_{\text{T}}^{\text{miss}}$ energy scale, and the uncertainties on the scale factors to correct the differences between the data and simulation in b- or c-tagging, lepton identification and isolation efficiencies. These total uncertainties from these sources are typically in range of 1–20%, depending on the signal regions.

The second set of systematic uncertainties has a larger impact on the prediction: the statistical uncertainties on the normalization are typically in range 2–10% while the effects of these uncertainties on the shape vary from 10–100%; the uncertainties related to the subtraction of other background sources in the dilepton sample range from range from 5% to 40%; the effect of the difference in the H_T shape has an average value of 10%; the uncertainty related to the trigger efficiency amounts to 5%.

4.2 Lost lepton estimation

The lost lepton background is predicted using a single-lepton (e or μ) control region. The combined prediction for $t\bar{t}$, W + jets and single top processes is obtained from data in each control region by applying a transfer factor that is determined from MC simulation and extrapolated to the signal region. The lost lepton background in the signal region i, $N_{SR_i}^{Pred}$, is predicted as:

$$N_{SR_i}^{Pred} = N_{CR_i}^{obs} \cdot (\frac{N_{SR_i}^{MC}}{N_{CR_i}^{MC}}). \tag{4}$$

where $N_{CR_i}^{MC}$ and $N_{SR_i}^{MC}$ are the number of simulate events in the single-lepton control sample and search region, respectively and $N_{CR_i}^{obs}$ is the number of observed events in the single-lepton control sample.

The same H_T, m_{CT}, N_{b-tags}, N_{c-tags}, N_{SV}, and E_T^{miss} binning as the search region is used in the single-lepton control sample. The normalization to data accounts for the kinematic modeling of all variables and the statistical uncertainty from the control region measurement is propagated to the uncertainty on the prediction.

Possible sources of systematic uncertainties on the predicted number of $t\bar{t}$, single top, and W + jets events in the search region are described next.

The $t\bar{t}$, single top, and W + jets admixture changes in different kinematic regions. A systematic uncertainty is derived to account for the variation of the transfer factor due to the relative composition of these processes. To account for this, we perform four closure tests: one for the non-compressed region and three tests for the compressed region. In the non-compressed region we start with a single-lepton control sample that has one b-tagged jet (which is nearly an equal mixture of $t\bar{t}$ and W + jets), and predict the event yield in the single-lepton control sample with two b-tagged jets (dominantly $t\bar{t}$) using the transfer factors obtained from simulation. The same procedure is applied to the compressed region, but this time we use zero b-tagged (one b- or c-tagged) single-lepton control sample to estimate the yield in the one b-tagged (two b- or c-tagged) control region. The deviation between the predicted and observed yields in this test is taken as a systematic uncertainty on the transfer factor.

The contamination from other SM processes, e.g, Drell-Yan and diboson in the single-lepton control sample is less than 2%. We do not subtract their contribution from the observed events in Eq. 4, but rather we assign a corresponding systematic uncertainty due to their contamination. The variation in the transfer factor, found after scaling the cross section by a factor of 50% for Drell-Yan and diboson processes, is taken as systematic uncertainty due to this contamination.

Table 4 provides a detailed breakdown of the various components of the systematic uncertainties in the non-compressed and compressed regions.

Table 4: Typical ranges for the different systematic uncertainties on the lost lepton background estimate.

Source	non-compressed region	compressed region
b-tag scale factor	12–25%	8–22%
c-tag scale factor	–	11-23%
Lepton scale factor	3–4%	3–4%
Isolated track	7%	7%
Transfer factor (statistical uncertainty)	5–60%	1–40%
Transfer factor (systematic uncertainty)	1-20%	15-25%
CR contamination	3–5%	3–10%

4.3 QCD multijet estimation

Due to the $\Delta\phi_{\text{min}}$ requirement, the QCD contribution is expected to be a small fraction of the total background for all signal regions in both the compressed and non-compressed regions. An estimate of this contribution is made by measuring the number of QCD multijet events in a QCD enriched control region and scaling this number by a transfer factor (T_{QCD}). The control region is identical to the search region, with the exception that the $\Delta\phi_{\text{min}}$ requirement is inverted. The transfer factor is found in a sideband region by measuring the ratio between the number of QCD multijet events with the standard and inverted $\Delta\phi_{\text{min}}$ requirement. The sideband is selected by $E_{\text{T}}^{\text{miss}} \in [200, 250]$ GeV.

Due to small QCD contribution in the standard $\Delta\phi_{\text{min}}$ region we determine T_{QCD} in the sideband region using simulation and validate it with data. The simulation models data well in both $\Delta\phi_{\text{min}}$ bins of the sideband region — the data and simulation ratio is consistent with one within 10% statistical uncertainty. We therefore take T_{QCD} from simulation, assuming 100% systematic uncertainty.

As T_{QCD} in the non-compressed region does not vary much as a function of $E_{\text{T}}^{\text{miss}}$, H_{T}, and m_{CT}, an inclusive H_{T} and m_{CT} bin is used in order to increase the statistical power of the sample used to extract the transfer factor.

In the compressed region T_{QCD} is obtained from sidebands requiring similar b-, c-tagged jet, and selected SV multiplicities as in the search region. Due to very low number of events in the sideband with exactly two b-tagged (c-tagged jets), the same T_{QCD} is used for both regions with one or two b-tagged (c-tagged) jets.

The statistical uncertainties on the observed number of events in the sideband and control regions, as well as the statistical and systematic uncertainties on the expected non-QCD events from simulation, are propagated as a systematic uncertainty in the final QCD prediction with typical values of 7-20%.

5 Results and Interpretation

The predicted SM background event yield and the number of events observed in data are summarized in Table 5 for the non-compressed search region, Tables 6, 7, 8 for the compressed search region, and in Fig. 4 for all search regions, using the methods defined in Section 4.

The data are consistent with the background expected from the SM processes. The result is interpreted as a cross section upper limit on top and bottom squark production, in the context of a simplified model (SMS) [46–49]. Two scenarios, known as T2bb and T2cc, are considered,

Table 5: Observed number of events and background prediction (individual, total) in the non-compressed region. The uncertainties shown combine the statistical and systematic components.

non-compressed region								
H_T [GeV]	m_{CT} [GeV]	bin	$Z \to \nu\nu$	Lost-Lepton	QCD	Rare	Total SM	Data
[200, 500]	[150, 250]	1	123±27	145±27	<0.7	8.8±4.4	278±40	275
	[250, 350]	2	130±26	125±29	$0.96^{+1.67}_{-0.96}$	9.8±4.9	266±40	292
	[350, 450]	3	28.5±9.1	31.6±7.2	$1.06^{+1.57}_{-1.06}$	1.87±0.93	63±12	57
	>450	4	0.64±0.57	0.56±0.46	<0.30	<0.2	1.21±0.79	2
[500,1000]	[150,250]	5	21.2±6.6	9.2±3.7	$0.85^{+1.08}_{-0.85}$	0.47±0.24	31.8±7.6	32
	[250, 350]	6	24.2±6.1	12.8±4.5	$0.99^{+1.3}_{-0.99}$	<0.2	37.9±7.8	27
	[350, 450]	7	14.3±3.5	6.1±2.1	$1.2^{+1.6}_{-1.2}$	0.47±0.24	22.2±4.4	30
	[450, 600]	8	19.1±6.2	8.6±2.3	$1.1^{+1.5}_{-1.1}$	<0.2	28.9±6.8	29
	>600	9	4.4±2.4	1.25±0.67	<0.46	<0.2	5.7±2.5	6
> 1000	[150, 250]	10	6.6±1.7	5.2±4.1	<0.23	<0.2	11.8±4.4	10
	[250, 350]	11	5.4±1.5	2.8±1.7	$0.37^{+0.53}_{-0.35}$	<0.2	8.6±2.3	9
	[350, 450]	12	2.71±0.82	3.2±1.9	$0.62^{+0.80}_{-0.62}$	<0.2	6.6±2.3	4
	[450, 600]	13	2.3±0.83	0.73±0.65	$0.64^{+0.82}_{-0.64}$	<0.2	3.7±1.3	3
	[600, 800]	14	1.08±0.57	0.12±0.15	<0.13	<0.2	1.22±0.61	0
	>800	15	2.1±1.4	0.38±0.40	<0.21	<0.2	2.5±1.5	0

Table 6: Observed number of events and background prediction (individual and total) in the compressed region with N_{b-tags} = 1,2. the uncertainties shown combine the statistical and systematic components.

compressed region								
E_T^{miss} [GeV]	H_T (b-tagged jets) [GeV]	Bin	$Z \to \nu\nu$	Lost-Lepton	QCD	Rare	Total SM	Data
N_{b-tags} =1								
[250, 300]	<100	1	555±92	1118±210	26^{+27}_{-26}	21±10	1720±232	1768
[300, 500]	<100	2	1100±133	1195±224	14^{+15}_{-14}	38±19	2348±262	2402
[500, 750]	<100	3	162±21	55±12	<0.33	6.7±3.5	224±25	211
[750, 1000]	<100	4	17.7±4.3	5.7±2.4	<0.15	<0.2	23.4±4.9	19
> 750	<100	5	3.6±1.6	0.51±0.50	<0.1	<0.2	4.1±1.7	5
N_{b-tags} =2								
[250, 300]	<100	6	6.9±2.8	51±12	$0.36^{+0.46}_{-0.36}$	0.47±0.23	59±12	70
[250, 300]	[100, 200]	7	12.9±4.5	120±25	$0.62^{+0.78}_{-0.62}$	<0.2	134±25	127
[300, 500]	<100	8	19.4±6.3	72±17	<0.2	1.36±0.68	92±18	77
[300, 500]	[100, 200]	9	34±10	151±31	< 0.2	1.35±0.67	188±32	161
> 500	<100	10	2.64±0.98	1.22±0.87	<0.1	<0.2	3.9±1.3	7
> 500	[100, 200]	11	8.7±2.9	5.1±2.3	<0.1	0.45±0.22	14.35±3.7	8

Table 7: Observed number of events and background prediction (individual and total) in the compressed region with $N_{\mathrm{c-tags}}$ = 1,2. The uncertainties shown combine the statistical and systematic components.

compressed region								
$E_{\mathrm{T}}^{\mathrm{miss}}$ [GeV]	H_{T} (c-tagged jets) [GeV]	Bin	$\mathrm{Z} \to \nu\nu$	Lost-Lepton	QCD	Rare	Total SM	Data
$N_{\mathrm{c-tags}}$ =1								
[250, 300]	<100	1	3022±481	3049±529	20^{+22}_{-20}	85±42	6177±717	6867
[300, 500]	<100	2	5852±685	3622±624	11^{+12}_{-11}	178±89	9664±931	10515
[500, 750]	<100	3	765±95	214±39	<0.2	22±11	1002±103	926
[750, 1000]	<100	4	67±13	16.2±3.9	<0.1	3.7±1.8	88±14	73
> 1000	<100	5	16.0±6.9	1.37±0.78	<0.1	0.45±0.22	17.8±7.1	18
$N_{\mathrm{c-tags}}$ =2								
[250, 300]	<100	6	145±33	198±42	$0.98^{+1.1}_{-0.98}$	4.1±2.1	348±54	364
[250, 300]	100, 200	7	199±25	238±46	4.3±4.7	7.8±3.9	449±53	508
[300, 500]	<100	8	293±39	229±45	0.81±0.91	9.7±4.8	532±60	547
[300, 500]	[100, 200]	9	489±55	323±59	1.5±1.7	19.3±9.6	833±81	874
[500, 750]	<100	10	44±13	23.4±7.2	<0.1	2.3±1.1	70±15	56
[500, 750]	[100, 200]	11	95±14	31.8±7.8	<0.1	3.7±1.8	130±16	102
> 750	<100	12	3.6±1.9	0.52±0.58	<0.1	<0.2	4.1±1.9	2
> 750	[100, 200]	13	6.7±2.6	2.9±1.6	<0.1	0.45±0.22	10.1±3.1	8

Table 8: Observed number of events and background prediction (individual and total) in the compressed region with $N_{\mathrm{b-tags}} + N_{\mathrm{c-tags}}$ = 0. The uncertainties shown combine the statistical and systematic components.

compressed region							
$E_{\mathrm{T}}^{\mathrm{miss}}$ [GeV]	Bin	$\mathrm{Z} \to \nu\nu$	Lost-Lepton	QCD	Rare	Total SM	Data
$N_{\mathrm{b-tags}} + N_{\mathrm{c-tags}} + N_{\mathrm{SV}}$ =0							
[300, 500]	1	10676±741	5398±925	148^{+165}_{-148}	320±160	16542±1207	17042
[500, 750]	2	1902±180	414±73	$1.4^{+2.1}_{-1.4}$	39±19	2358±196	2028
[750, 1000]	3	143±21	31.2±6.6	<0.45	6.1±3.1	181±22	171
[1000, 1250]	4	42±16	5.9±2.8	<0.03	0.47±0.23	49±16	33
> 1250	5	5.1±5.7	2.3±1.6	$0.09^{+0.17}_{-0.09}$	0.92±0.46	8.4±6.0	9
$N_{\mathrm{b-tags}} + N_{\mathrm{c-tags}}$ =0, $N_{\mathrm{SV}} > 0$							
[250, 300]	6	169±22	179±36	$4.5^{+5.1}_{-4.5}$	3.7±1.9	357±43	331
[300, 500]	7	303±37	210±41	$2.9^{+3.3}_{-2.9}$	6.9±3.4	523±57	509
[500, 750]	8	46.6±6.2	15.1±4.8	$0.03^{+0.13}_{-0.03}$	1.40±0.70	64.2±7.8	52
[750, 1000]	9	5.7±1.2	0.73±0.59	<0.1	<0.2	6.5±1.3	3
> 1000	10	1.5±1.1	0.07±0.10	<0.2	0.45±0.22	2.0±1.1	0

in which bottom (top) squarks are produced in pairs, with each decaying to a bottom (charm) quark and an invisible massive particle.

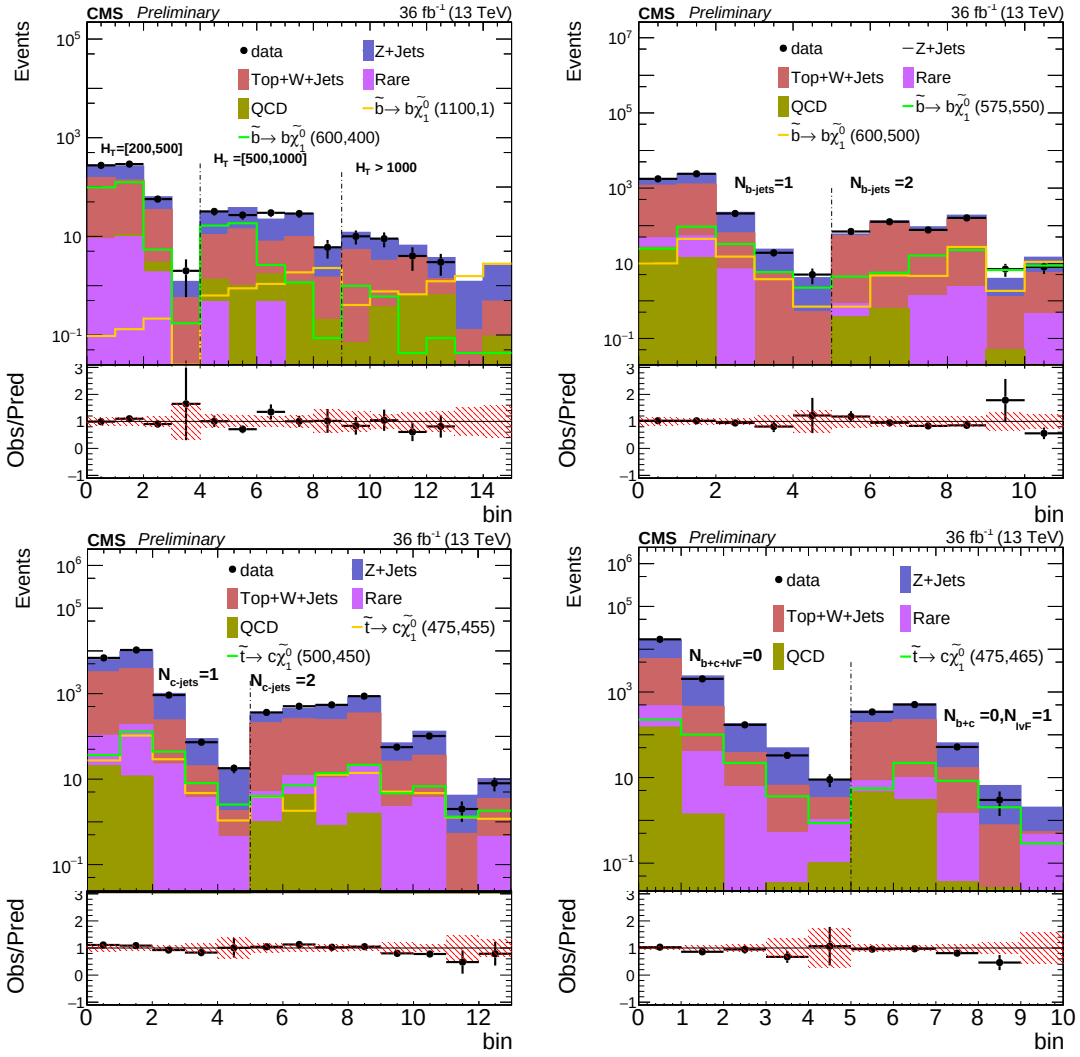

Figure 4: Yields in the signal regions targeting the non-compressed (top left) and compressed (top right: $N_{\mathrm{b-tags}}$ =1,2, bottom left: $N_{\mathrm{c-tags}}$ =1,2, bottom right: $N_{\mathrm{b-tags}}$ +$N_{\mathrm{c-tags}}$ =0) scenarios. Data are shown as black points. The background predictions are represented by the stacked, filled histograms. The expected yields for two signal models are also shown. The lower panels show the ratio of data over total background prediction in each signal region.

The 95% confidence level (CL) upper limits on SUSY production cross sections are calculated using a modified frequentist approach with the $\mathrm{CL_S}$ criterion [50–52] and asymptotic results for the test statistic [53].

The 49 signal bins in $E_{\mathrm{T}}^{\mathrm{miss}}$, H_{T}, m_{CT}, b- or c-tagged jet multiplicities, and selected SV, are used as statistically independent channels in the limit calculation, and the correlations between all the systematic uncertainties in different bins are taken into account.

The dominant systematic uncertainties on the signal yield predictions are accounted for as follows: the luminosity determination (2.6%), the signal acceptance and efficiency arising from the jet energy corrections (5%); renormalization and factorization scale (5%); ISR recoil (5%–20%); trigger efficiency (2%); b- and c-tagging efficiency (5%–30%); and selected SV efficiency (14–

50%). The statistical uncertainty, which is calculated point by point, varies from a few percent to 100% and is not correlated with signal systematic uncertainties. While the uncertainties on the b- and c-tagged jet and lepton efficiency corrections in simulation are correlated between different processes and search bins, the uncertainties on transfer factors are treated as fully uncorrelated. For the signal, all systematic uncertainties are correlated between the different search regions.

Figure 5 right plot shows the expected and observed 95% confidence level upper limits on the bottom squark cross sections in the $(m_{\tilde{b}}, m_{LSP})$ plane. The cross section is determined at NLO in the strong coupling constant and includes the resummation of soft gluon emission at the accuracy of next-to-leading-log (NLL) level [54–58]. The one standard deviation experimental (theoretical) uncertainty is shown around the expected (observed) exclusion curve. The theoretical error is based on changing the renormalization and factorization scales by a factor of two to illustrate the sensitivity of the exclusion to the signal cross section uncertainty. For small LSP masses, the expected limit excludes bottom squark masses below 1225 GeV at 95% confidence level.

Figure 5 right plot shows the expected and observed 95% confidence level upper limits on the top squark cross sections in the $(m_{\tilde{t}}, m_{LSP})$ plane. Top squarks with masses below 525 GeV are excluded if the mass splitting between a top squark and an LSP is close to 10 GeV.

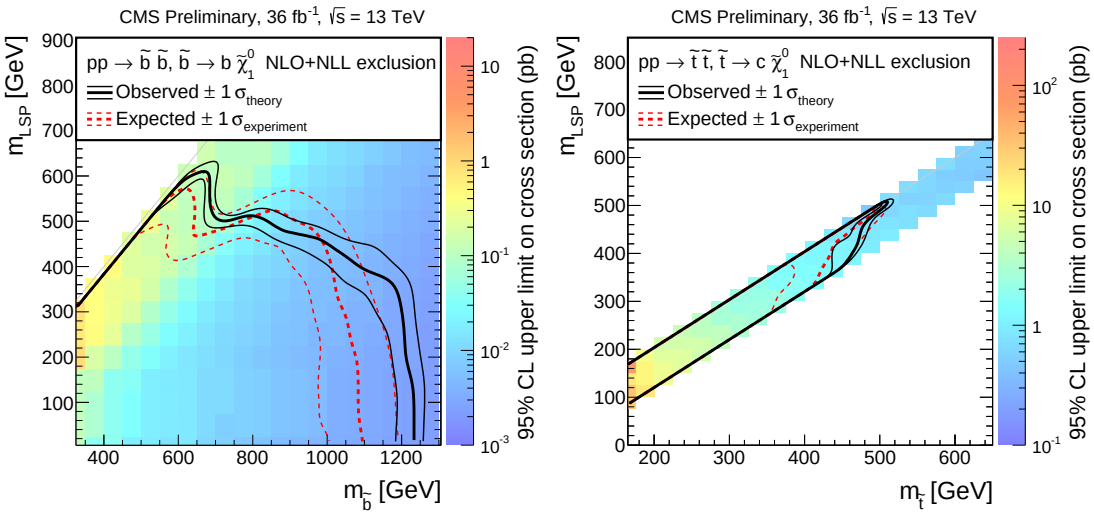

Figure 5: The 95% CL limits on the cross section, assuming 100% BR for the decay of the top squark shown in the legend (left). The combined 95% CL exclusion limits for top squark pair production assuming 100% branching fraction to the decay $\tilde{t} \to c\tilde{\chi}_1^0$. The mass limits are shown as a black line for the observed limit and as a red line for the expected limit.

To facilitate re-interpretation, the covariance matrices for the background estimates in the compressed and non-compressed search regions are provided and given in Appendix A.

6 Conclusion

A search for pair production of bottom and top squarks is reported, based on a data sample of pp collisions collected with the CMS detector at $\sqrt{s}$ = 13 TeV in 2016, corresponding to an integrated luminosity of 36 fb^{-1}. Final states with two, three, and four jets, two of which originate from b or c quarks, and significant $E_{\mathrm{T}}^{\mathrm{miss}}$ have been analyzed. The search has been performed

in exclusive binned signal regions defined by the number of jets identified as originating from a b or c quark, missing energy, scalar sum of the jets p_{T}, and the contransverse mass. The standard model backgrounds per bin have been estimated from data control samples. We observe no excess above the SM predictions. Exclusion limits are set at the 95% CL on the simplified model production of a pair of bottom (top) squarks, with each bottom (top) squark decaying to a bottom (charm) quark and the lightest neutralino. The production of bottom squarks with masses up to 1225 GeV is excluded at 95% confidence level for neutralino masses less than 100 GeV. Top squarks with masses below 525 GeV are excluded if mass splitting between a top squark and an LSP is close to 10 GeV.

References

[1] G. 't Hooft, "Naturalness, chiral symmetry, and spontaneous chiral symmetry breaking", *NATO Sci. Ser. B* **59** (1980) 135.

[2] E. Witten, "Dynamical breaking of supersymmetry", *Nucl. Phys. B* **188** (1981) 513, doi:10.1016/0550-3213(81)90006-7.

[3] M. Dine, W. Fischler, and M. Srednicki, "Supersymmetric technicolor", *Nucl. Phys. B* **189** (1981) 575, doi:10.1016/0550-3213(81)90582-4.

[4] S. Dimopoulos and S. Raby, "Supercolor", *Nucl. Phys. B* **192** (1981) 353, doi:10.1016/0550-3213(81)90430-2.

[5] S. Dimopoulos and H. Georgi, "Softly broken supersymmetry and SU(5)", *Nucl. Phys. B* **193** (1981) 150, doi:10.1016/0550-3213(81)90522-8.

[6] R. K. Kaul and P. Majumdar, "Cancellation of quadratically divergent mass corrections in globally supersymmetric spontaneously broken gauge theories", *Nucl. Phys. B* **199** (1982) 36, doi:10.1016/0550-3213(82)90565-X.

[7] J. Wess and B. Zumino, "Supergauge transformations in four-dimensions", *Nucl. Phys. B* **70** (1974) 39, doi:10.1016/0550-3213(74)90355-1.

[8] G. R. Farrar and P. Fayet, "Phenomenology of the Production, Decay, and Detection of New Hadronic States Associated with Supersymmetry", *Phys. Lett. B* **76** (1978) 575, doi:10.1016/0370-2693(78)90858-4.

[9] C. Boehm, A. Djouadi, and M. Drees, "Light scalar top quarks and supersymmetric dark matter", *Phys. Rev. D* **62** (2000) 035012, doi:10.1103/PhysRevD.62.035012, arXiv:hep-ph/9911496.

[10] C. Balázs, M. Carena, and C. E. M. Wagner, "Dark matter, light stops and electroweak baryogenesis", *Phys. Rev. D* **70** (2004) 015007, doi:10.1103/PhysRevD.70.015007, arXiv:hep-ph/403224.

[11] G. Jungman, M. Kamionkowski, and K. Griest, "Supersymmetric dark matter", *Phys. Rept.* **267** (1996) 195, doi:10.1016/0370-1573(95)00058-5, arXiv:hep-ph/9506380.

[12] CMS Collaboration, "The CMS experiment at the CERN LHC", *JINST* **3** (2008) S08004, doi:10.1088/1748-0221/3/08/S08004.

[13] A. Delgado et al., "The light stop window", *Eur. Phys. J.* **C73** (2013), no. 3, 2370, doi:10.1140/epjc/s10052-013-2370-5, arXiv:1212.6847.

[14] ATLAS Collaboration, "Search for a supersymmetric partner to the top quark in final states with jets and missing transverse momentum at $\sqrt{s} = 7$ TeV with the ATLAS detector", *Phys. Rev. Lett.* **109** (2012) 211802, doi:10.1103/PhysRevLett.109.211802, arXiv:1208.1447.

[15] ATLAS Collaboration, "Search for direct top squark pair production in final states with one isolated lepton, jets, and missing transverse momentum in $\sqrt{s} = 7$ TeV pp collisions using 4.7 fb^{-1} of ATLAS data", *Phys. Rev. Lett.* **109** (2012) 211803, doi:10.1103/PhysRevLett.109.211803, arXiv:1208.2590.

[16] ATLAS Collaboration, "Search for a heavy top-quark partner in final states with two leptons with the ATLAS detector at the LHC", *JHEP* **11** (2012) 094, doi:10.1007/JHEP11(2012)094, arXiv:1209.4186.

[17] ATLAS Collaboration, "Search for direct top-squark pair production in final states with two leptons in pp collisions at $\sqrt{s} = 8$ TeV with the ATLAS detector", *JHEP* **06** (2014) 124, doi:10.1007/JHEP06(2014)124, arXiv:1403.4853.

[18] ATLAS Collaboration, "Search for direct third-generation squark pair production in final states with missing transverse momentum and two b-jets in $\sqrt{s} = 8$ TeV pp collisions with the ATLAS detector", *JHEP* **10** (2013) 189, doi:10.1007/JHEP10(2013)189, arXiv:1308.2631.

[19] ATLAS Collaboration, "Measurement of Spin Correlation in Top-Antitop Quark Events and Search for Top Squark Pair Production in pp Collisions at $\sqrt{s} = 8$ TeV Using the ATLAS Detector", *Phys. Rev. Lett.* **114** (2015) 142001, doi:10.1103/PhysRevLett.114.142001, arXiv:1412.4742.

[20] ATLAS Collaboration, "Search for pair-produced third-generation squarks decaying via charm quarks or in compressed supersymmetric scenarios in pp collisions at $\sqrt{s} = 8$ TeV with the ATLAS detector", *Phys. Rev. D* **90** (2014) 052008, doi:10.1103/PhysRevD.90.052008, arXiv:1407.0608.

[21] ATLAS Collaboration, "ATLAS Run 1 searches for direct pair production of third-generation squarks at the Large Hadron Collider", *Eur. Phys. J. C* **75** (2015) 510, doi:10.1140/epjc/s10052-015-3726-9, arXiv:1506.08616.

[22] CMS Collaboration, "Search for top-squark pair production in the single-lepton final state in pp collisions at $\sqrt{s}$ = 8 TeV", *Eur. Phys. J. C* **73** (2013) 2677, doi:10.1140/epjc/s10052-013-2677-2, arXiv:1308.1586.

[23] CMS Collaboration, "Search for supersymmetry in hadronic final states with missing transverse energy using the variables α_{T} and b-quark multiplicity in pp collisions at $\sqrt{s} = 8$ TeV", *Eur. Phys. J. C* **73** (2013) 2568, doi:10.1140/epjc/s10052-013-2568-6, arXiv:1303.2985.

[24] CMS Collaboration, "Search for supersymmetry using razor variables in events with b-tagged jets in pp collisions at $\sqrt{s} = 8$ TeV", *Phys. Rev. D* **91** (2015) 052018, doi:10.1103/PhysRevD.91.052018, arXiv:1502.00300.

[25] CMS Collaboration, "Searches for third-generation squark production in fully hadronic final states in proton-proton collisions at $\sqrt{s} = 8$ TeV", *JHEP* **06** (2015) 116, doi:10.1007/JHEP06(2015)116, arXiv:1503.08037.

[26] CMS Collaboration, "Search for direct pair production of supersymmetric top quarks decaying to all-hadronic final states in pp collisions at $\sqrt{s}$ = 8 TeV", *Eur. Phys. J. C* **76** (2016) 460, doi:10.1140/epjc/s10052-016-4292-5, arXiv:1603.00765.

[27] CMS Collaboration, "Particle Flow Event Reconstruction in CMS and Performance for Jets, Taus and MET", CMS Physics Analysis Summary CMS-PAS-PFT-09-001, 2009.

[28] CMS Collaboration, "Commissioning of the Particle-Flow Reconstruction in Minimum-Bias and Jet Events from pp Collisions at 7 TeV", CMS Physics Analysis Summary CMS-PAS-PFT-10-002, 2010.

[29] CMS Collaboration, "Commissioning of the particle-flow event reconstruction with leptons from J/Psi and W decays at 7 TeV", CMS Physics Analysis Summary CMS-PAS-PFT-10-003, 2010.

[30] M. Cacciari, P. Salam, and G. Soyez, "The anti-kt jet clustering algorithm", *JHEP* **08** (2008) 063, doi:10.1088/1126-6708/2008/04/063.

[31] M. Cacciari, M. Salam, P. Gavin, and G. Soyez, "Pileup subtraction using jet areas", *Phys. Lett. B* **659** (2007) 119, doi:10.1016/j.physletb.2007.09.077, arXiv:0707.1378.

[32] CMS Collaboration, "Performance of the CMS missing transverse momentum reconstruction in pp data at $\sqrt{s}$ = 8 TeV", *JINST* **10** (2015) P02006, doi:10.1088/1748-0221/10/02/P02006, arXiv:1411.0511.

[33] CMS Collaboration, "Performance of CMS muon reconstruction in pp collision events at $\sqrt{s} = 7$ TeV", *JINST* **7** (2012) P10002, doi:10.1088/1748-0221/7/10/P10002, arXiv:1206.4071.

[34] CMS Collaboration, "Identification of b-quark jets with the CMS experiment", *JINST* **8** (2013) P04013, doi:10.1088/1748-0221/8/04/P04013, arXiv:1211.4462.

[35] CMS Collaboration Collaboration, "Identification of c-quark jets at the CMS experiment", Technical Report CMS-PAS-BTV-16-001, CERN, Geneva, 2016.

[36] J. Alwall et al., "MADGRAPH 5 : Going Beyond", *JHEP* **06** (2011) 128, doi:10.1007/JHEP06(2011)128, arXiv:1106.0522.

[37] J. Alwall et al., "The automated computation of tree-level and next-to-leading order differential cross sections, and their matching to parton shower simulations", *JHEP* **07** (2014) 079, doi:10.1007/JHEP07(2014)079, arXiv:1405.0301.

[38] S. M. T. Sjostrand and P. Z. Skands, "A Brief Introduction to PYTHIA 8.1", *Comput. Phys. Commun.* **178** (2008) 852–867, doi:10.1016/j.cpc.2008.01.036.

[39] GEANT4 Collaboration, "GEANT4 @ simulation toolkit", *Nucl. Instrum. Meth. A* **506** (2003) 250, doi:10.1016/S0168-9002(03)01368-8.

[40] CMS Collaboration, "Fast simulation of the CMS detector", *J. Phys. Conf. Ser.* **219** (2010) doi:doi:10.1088/1742-6596/219/3/032053.

[41] CMS Collaboration, "Pileup subtraction using jet areas", *Phys. Lett. B* **659** (2008) 119–126, doi:10.1016/j.physletb.2007.09.077, arXiv:0707.1378.

[42] D. Tovey, "Supersymmetric particle mass measurement with boost-corrected constransverse mass", *JHEP* **03** (2010) doi:10.1007/JHEP03(2010)030.

[43] G. Polesello and D. Tovey, "On measuring the masses of pair-produced semi-invisibly decaying particles at hadron colliders", *JHEP* **04** (2008) doi:10.1088/1126-6708/2008/04/034.

[44] CMS Collaboration Collaboration, "Identification of double-b quark jets in boosted event topologies", Technical Report CMS-PAS-BTV-15-002, CERN, Geneva, 2016.

[45] Particle Data Group Collaboration, "Review of Particle Physics", *Chin. Phys. C* **38** (2014) 090001, doi:10.1088/1674-1137/38/9/090001.

[46] CMS Collaboration, "Interpretation of Searches for Supersymmetry with simplified Models", *Phys. Rev. D* **88** (2013), no. 5, 052017, doi:10.1103/PhysRevD.88.052017, arXiv:1301.2175.

[47] J. Alwall, P. Schuster, and N. Toro, "Simplified Models for a First Characterization of New Physics at the LHC", *Phys. Rev. D* **79** (2009) doi:10.1103/PhysRevD.79.075020.

[48] J. Alwall, M.-P. Le, M. Lisanti, and et al, "Model-Independent Jets plus Missing Energy Searches", *Phys. Rev. D* **79** (2009) doi:10.1103/PhysRevD.79.015005.

[49] LHC New Physics Working Group Collaboration, "Simplified Models for LHC New Physics Searches", *J. Phys. G* **39** (2012) 105005, doi:10.1088/0954-3899/39/10/105005, arXiv:1105.2838.

[50] A. L. Read, "Presentation of search results: the CL s technique", *J. Phys. G* **28** (2002) 2693, doi:10.1088/0954-3899/28/10/313.

[51] T. Junk, "Confidence level computation for combining searches with small statistics", *Nucl. Instr. and Meth. A* **434** (1999) 435, doi:10.1016/S0168-9002(99)00498-2.

[52] ATLAS and CMS Collaboration, "Procedure for the LHC Higgs boson search combination in Summer 2011",.

[53] G. Cowan, K. Cranmer, E. Gross, and O. Vitells, "Asymptotic formulae for likelihood-based tests of new physics", *Eur. Phys. J.* **C71** (2011) 1554, doi:10.1140/epjc/s10052-011-1554-0, 10.1140/epjc/s10052-013-2501-z, arXiv:1007.1727. [Erratum: Eur. Phys. J.C73,2501(2013)].

[54] A. Kulesza and L. Motyka, "Threshold resummation for squark-antisquark and 645 gluino-pair production at the LHC", *Phys. Rev. Lett.* **102** (2009) 111802, doi:doi:10.1103/PhysRevLett.102.111802.

[55] A. Kulesza and L. Motyka, "Soft gluon resummation for the production of gluino-gluino and squark-antisquark pairs at the LHC", *Phys. Rev. Lett.* **80** (2009) 095004, doi:doi:10.1103/PhysRevLett.80.095004.

[56] W. Beenakker and et al., "Soft-gluon resummation for squark and gluino hadroproduction", *JHEP* **12** (2009) 041, doi:doi:10.1088/1126-6708/2009/12/041.

[57] W. Beenakker and et al., "Squark and gluino hadroproduction", *Int. J. Mod. Phys. A* **26** (2011) 2637, doi:doi:10.1142/S0217751X11053560.

[58] M. Kramer and et al., "Supersymmetry production cross sections in pp collisions at $\sqrt{s}$ =7 TeV", (2012). arXiv:1206.2892.

A Covariance Matrix

The covariance and correlation matrices for the background estimates in the compressed and non-compressed search regions are shown in Figure 6. The bin number in the compressed region is the same as it is shown in Table 5 and in the compressed region it is shown Table 9.

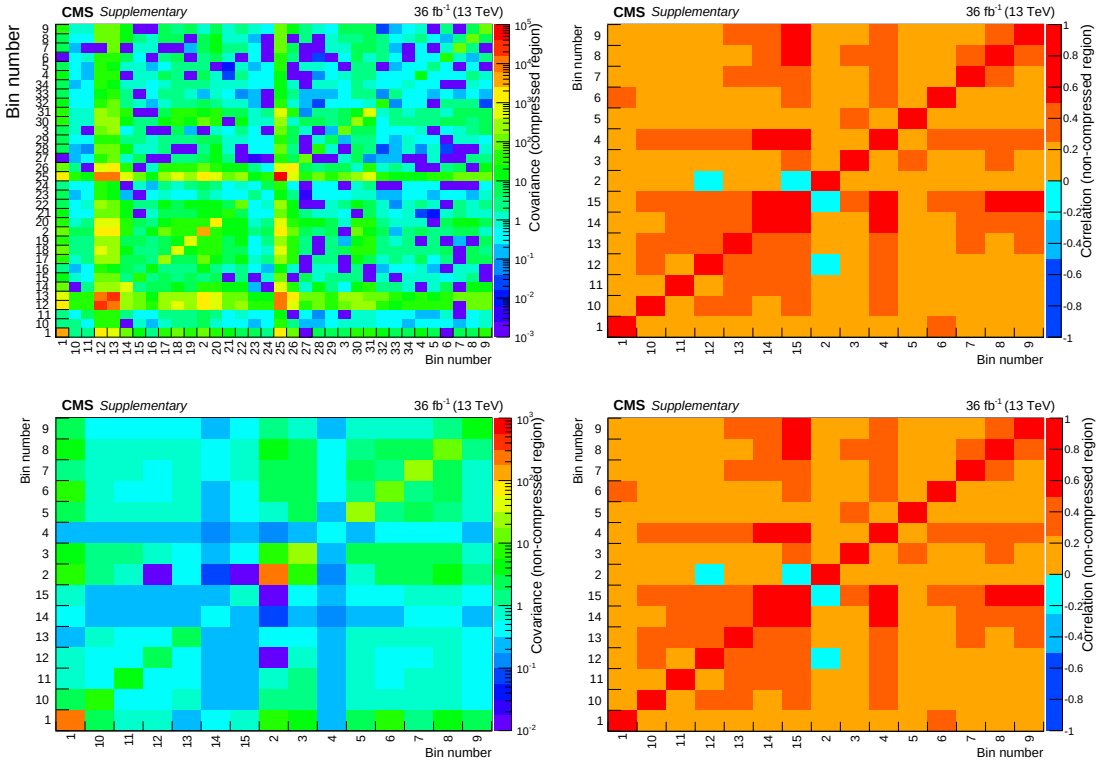

Figure 6: The covariance and correlation matrices for the estimated backgrounds in the compressed and non-compressed search regions.

Table 9: The bin number and definition in the compressed search region.

compressed region			
$N_{\mathrm{b-tags}}$,$N_{\mathrm{c-tags}}$,N_{SV}	$E_{\mathrm{T}}^{\mathrm{miss}}$ [GeV]	H_{T} (b- or c-tagged jets) [GeV]	bin
$N_{\mathrm{b-tags}}$ =1	[250, 300]	<100	1
	[300, 500]	<100	2
	[500, 750]	<100	3
	[750, 1000]	<100	4
	>1000	<100	5
$N_{\mathrm{b-tags}}$ =2	$\in$ [250, 300]	<100	6
		[100, 200]	7
	$\in$ [300, 500]	<100	8
		[100, 200]	9
	>500	<100	10
		[100, 200]	11
$N_{\mathrm{c-tags}}$ =1	$\in$ [250, 300]	<100	12
	[300, 500]	<100	13
	[500, 750]	<100	14
	[750, 1000]	<100	15
	>1000	<100	16
$N_{\mathrm{c-tags}}$ =2	$\in$ [250, 300]	<100	17
		[100, 200]	18
	$\in$ [300, 500]	<100	19
		[100, 200]	20
	$\in$ [500, 750]	<100	21
		[100, 200]	22
	>750	<100	23
		[100, 200]	24
$N_{\mathrm{b-tags}}$ +$N_{\mathrm{c-tags}}$ =0,N_{SV} >0	$\in$ [250, 300]	-	25
	[300, 500]	-	26
	[500, 750]	-	27
	[750, 1000]	-	28
	>1000	-	29
$N_{\mathrm{b-tags}}$ +$N_{\mathrm{c-tags}}$ +N_{SV} =0	$\in$ [300, 500]	-	30
	[500, 750]	-	31
	[750, 1000]	-	32
	[1000, 1250]	-	33
	>1250	-	34